

Measurement of the internal magnetic field in the correlated iridates Ca_4IrO_6 , $\text{Ca}_5\text{Ir}_3\text{O}_{12}$, $\text{Sr}_3\text{Ir}_2\text{O}_7$ and Sr_2IrO_4

I. Franke,¹ P. J. Baker,^{1,2} S. J. Blundell,¹ T. Lancaster,¹ W. Hayes,¹ F. L. Pratt,² and G. Cao³

¹*Oxford University Department of Physics, Clarendon Laboratory,
Parks Road, Oxford OX1 3PU, United Kingdom*

²*ISIS Pulsed Neutron and Muon Source, STFC Rutherford Appleton Laboratory,
Harwell Science and Innovation Campus, Didcot, Oxfordshire, OX11 0QX, United Kingdom*

³*Department of Physics and Astronomy, University of Kentucky, Lexington, KY 40506*

(Dated: June 13, 2018)

Oxides containing iridium ions display a range of magnetic and conducting properties that depend on the delicate balance between interactions and are controlled, at least in part, by the details of the crystal architecture. We have used muon-spin rotation (μSR) to study the local field in four iridium oxides, Ca_4IrO_6 , $\text{Ca}_5\text{Ir}_3\text{O}_{12}$, $\text{Sr}_3\text{Ir}_2\text{O}_7$ and Sr_2IrO_4 , which show contrasting behavior. Our μSR data on Ca_4IrO_6 and $\text{Ca}_5\text{Ir}_3\text{O}_{12}$ are consistent with conventional antiferromagnetism where quasistatic magnetic order develops below $T_N = 13.85(6)$ K and $7.84(7)$ K respectively. A lower internal field is observed for $\text{Ca}_5\text{Ir}_3\text{O}_{12}$, as compared to Ca_4IrO_6 reflecting the presence of both Ir^{4+} and Ir^{5+} ions, resulting in a more magnetically dilute structure. Muon precession is only observed over a restricted range of temperature in $\text{Sr}_3\text{Ir}_2\text{O}_7$, while the Mott insulator Sr_2IrO_4 displays more complex behavior, with the μSR signal containing a single, well-resolved precession signal below $T_N = 230$ K, which splits into two precession signals at low temperature following a reorientation of the spins in the ordered state.

I. INTRODUCTION

Transition metal oxides have attracted widespread interest in recent years, driven partly by the observation of high temperature superconductivity in cuprates, colossal magnetoresistance in manganites and p-wave superconductivity in ruthenates^{1,2}. A wide variety of behavior can be expected since the transition metal ion can be any one of the 3d, 4d or 5d series and the possible crystal architectures that can be synthesized include chains, ladders, square layers, triangular layers, kagome layers, pyrochlore lattices and many more. The 5d series has received the least attention but the extended nature of the 5d orbitals leads to large crystal field energies³. The spin-orbit interaction is also strong, owing to the large atomic number, and these competing energy scales are likely to open up new possibilities for their magnetic behavior.

The iridium ion is a particularly attractive candidate for study because Ir^{4+} ($5d^5$) is an $S = \frac{1}{2}$ species and iridates display a wide variety of unusual characteristics. For example, Ca_4IrO_6 and $\text{Ca}_5\text{Ir}_3\text{O}_{12}$ are antiferromagnetically ordered at low temperature but exhibit weak ferromagnetism due to spin canting^{3,4}. $\text{Ca}_5\text{Ir}_3\text{O}_{12}$ exhibits a more complex partial spin ordering due to the presence of both Ir^{4+} and Ir^{5+} ions³. These two compounds have a large value of the ratio θ/T_N where θ is the Curie-Weiss temperature (see Table I) demonstrating the presence of competing interactions. $\text{Sr}_3\text{Ir}_2\text{O}_7$ is a weak ferromagnet showing complicated crossovers in its magnetic behaviour that have not yet been explained at the microscopic level⁵. Sr_2IrO_4 is a Mott insulator driven from the metallic state by the spin-orbit coupling to a $J_{\text{eff}} = \frac{1}{2}$ state^{6,7}. It is also a weak ferromagnet, shows a novel magnetoelectric state with a so far unex-

plained magnetic transition^{8,9} and has even been suggested as a candidate for high-temperature superconductivity if doped¹⁰.

In order to study systematically the dependence of local magnetic properties on crystal architecture we have used muon spin rotation (μSR) to investigate the microscopic magnetism and the critical behavior of each of these compounds. The nature of the muon spin rotation technique makes it very sensitive to the local magnetic environment, and especially to short-range magnetic order. We find a comparatively conventional development of the internal magnetic field in Ca_4IrO_6 with some more complex features in $\text{Ca}_5\text{Ir}_3\text{O}_{12}$. Compared to these the results for $\text{Sr}_3\text{Ir}_2\text{O}_7$ and Sr_2IrO_4 reveal very different behavior. Two magnetic transitions are evident in our data for $\text{Sr}_3\text{Ir}_2\text{O}_7$, while in the Mott insulator Sr_2IrO_4 we observe the development of spin reorientation at low temperature.

II. EXPERIMENTAL METHODS

Small crystallites of the materials were grown in Pt crucibles using self-flux techniques from off-stoichiometric quantities of IrO_2 , SrCO_3 or CaCO_3 , and SrCl_2 or CaCl_2 . These mixtures were heated to 1480°C in Pt crucibles, fired for 20 h and slowly cooled at $3^\circ\text{C}/\text{hour}$ to lower temperatures (1440°C for $\text{Sr}_3\text{Ir}_2\text{O}_7$, for example). Crystal structures of all single crystals studied were determined at 90 K and 295 K using a Nonius Kappa CCD X-Ray Diffractometer and Mo K(alpha) radiation. Chemical compositions of the single crystals were determined using energy dispersive X-ray analysis (EDX)

Zero-field μSR measurements¹⁴ were made using the General Purpose Surface (GPS) muon spectrometer at

	space group	μ_{eff} (μ_{B} /f.u.)	θ (K)	T_{N} (K)	$ \theta/T_{\text{N}} $	α	β	$\nu_1(0)$ (MHz)	$\nu_2(0)$ (MHz)
Ca_4IrO_6	$\text{R}\bar{3}\text{c}$	1.76 [11]	-54 [12]	13.95(6)	3.8(2)	4.2(3)	0.37(1)	8.29(3)	4.39(4)
$\text{Ca}_5\text{Ir}_3\text{O}_{12}$	$\text{P}\bar{6}2\text{m}$	1.5 [4]	-280 [3]	7.84(7)	35.7(1)	2.8(5)	0.40(6)	1.30(2)	-
$\text{Sr}_3\text{Ir}_2\text{O}_7$	I4/mmm	0.69 [5]	-17 [5]	285	0.06	-	-	-	-
Sr_2IrO_4	$\text{I}4_1/\text{acd}$	0.33 [13]	251 [13]	230.4(3)	1.08(2)	0.98(4)	0.21(1)	2.93(1)	-

TABLE I: Properties of the four compounds studied and parameters extracted from the fits presented here. The values of T_{N} are from this work, except for $\text{Sr}_3\text{Ir}_2\text{O}_7$, which is taken from Ref. 5.

the Swiss Muon Source. Each sample was wrapped in 25 μm silver foil and mounted on a silver backing plate. Spin-polarized positive muons are implanted in the target sample, where the muon usually occupies a position of high electronegativity in the crystal. The observed property in the experiment is the time-evolution of the muon-spin polarization, which is proportional to the positron asymmetry function $A(t)$ and depends on the local magnetic field B at the muon stopping site¹⁴. In these polycrystalline samples the internal magnetic field will be randomly orientated with respect to the initial muon polarization. Because of this we can expect that in a fully ordered magnet $\frac{2}{3}$ of the signal will be due to oscillations about the magnetic field perpendicular to the muon spin and $\frac{1}{3}$ will be relaxation due to the dynamic magnetic fluctuations parallel to the muon spin direction¹⁴.

III. Ca_4IrO_6 AND $\text{Ca}_5\text{Ir}_3\text{O}_{12}$

Ca_4IrO_6 has a rhombohedral structure, in which 1D chains of IrO_6 octahedra alternate with CaO_6 trigonal prisms^{3,12}. In contrast $\text{Ca}_5\text{Ir}_3\text{O}_{12}$ has a triangular lattice and a hexagonal structure^{4,15} and, unusually amongst iridates, in addition to Ir^{4+} it also includes Ir^{5+} ions. In

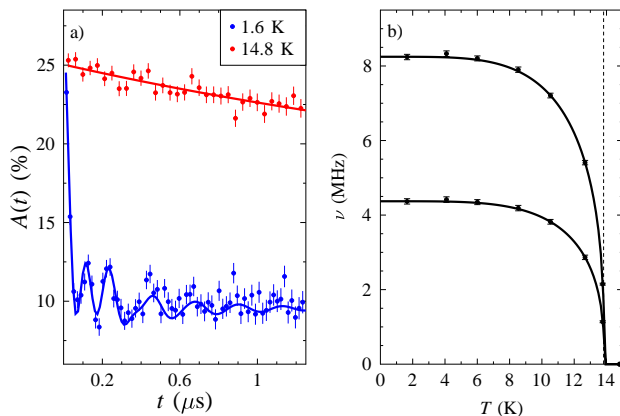


FIG. 1: (Color online) (a) Raw data for Ca_4IrO_6 above and below the magnetic phase transition. The low temperature data are fitted with two oscillating components as described by Eq. (1). (b) Precession frequencies ν_1 and ν_2 for the ordered state.

a cubic crystal field Ir^{5+} is in a $S = 0$ state^{16,17}, but in a rhombohedral or hexagonal environment the sizeable spin-orbit coupling may modify the level scheme. In spite of these differences both structures lead to the formation of spin chains perpendicular to a triangular lattice, promoting the occurrence of frustration.

Both compounds are insulators (below 300K for $\text{Ca}_5\text{Ir}_3\text{O}_{12}$) and exhibit antiferromagnetic order. The transition temperature for Ca_4IrO_6 was reported^{3,12} to be in the range of 12–16 K. $\text{Ca}_5\text{Ir}_3\text{O}_{12}$ is found to order into an antiferromagnetic state below 7.8 K^{3,4}.

Example data for Ca_4IrO_6 above and below the transition are shown in Fig. 1(a). In the paramagnetic phase the signal is described by a single exponential relaxation and below T_{N} we observe two well-defined precession frequencies along with a fast relaxing component at early times. The data in this regime may be parametrized using the equation:

$$\begin{aligned}
 A(t) = & A_1 \exp(-\lambda_1 t) \cos(2\pi\nu_1 t) \\
 & + A_2 \exp(-\lambda_2 t) \cos(2\pi\nu_2 t) \\
 & + A_3 \exp(-\Lambda t), + A_{\text{bg}}
 \end{aligned}
 \quad (1)$$

where A_i are the amplitudes of the components, λ_i are the corresponding relaxation rates, ν_i are the precession frequencies, and Λ is the relaxation rate of the fast-relaxing component. The constant A_{bg} accounts for muons stopped outside the sample as well as the expected one-third contributions arising from muon-spin components directed parallel to the local magnetic field. A satisfactory fit to the data could be obtained by fixing A_1 , A_2 , A_3 , λ_1 and λ_2 to temperature-independent values (4.02%, 1.37%, 11.2%, 5.03 MHz and 1.55 MHz respectively) and allowing ν_1 and ν_2 to vary in a fixed proportion $\nu_2/\nu_1 = 0.53$ (a ratio determined to better than 4% accuracy by first allowing them to vary independently). In addition, the large relaxation rate Λ was found to scale as ν_1^2 and reaches 22 MHz at 1.5 K. We deduce that there are two independent muon sites which experience a quasistatic local field (leading to the oscillatory components) and a further site at which the muon spin relaxes in a manner dominated by the magnitude of the local field (leading to the fast-relaxing component). The fast-relaxing component observed below the magnetic ordering temperature probably reflects a class of muon site at which the local field is large but where there exists some degree of spatial or temporal disorder. The

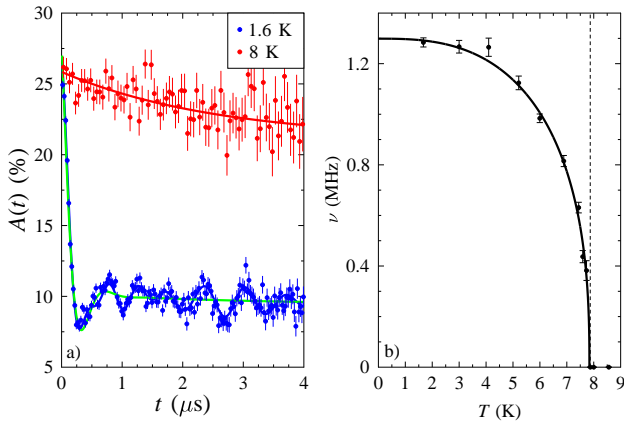


FIG. 2: (Color online) (a) Raw data for $\text{Ca}_5\text{Ir}_3\text{O}_{12}$ above and below the magnetic phase transition. The data below the transition is fitted with a single frequency (green) and a five frequency (blue) fit. (b) Precession frequency extracted from a single frequency fit to the $\text{Ca}_5\text{Ir}_3\text{O}_{12}$ data.

results of fitting the frequency ν_1 are illustrated in Fig. 1 (b).

The temperature dependence of ν_1 was fitted to the phenomenological form

$$\nu_1(T) = \nu_1(0)[1 - (T/T_N)^\alpha]^\beta. \quad (2)$$

The parameters extracted were: $T_N = 13.85(6)$ K, $\nu_1(0) = 8.29(3)$ MHz, $\alpha = 4.2(3)$, and $\beta = 0.37(1)$, and this value of β is consistent with a typical three-dimensional magnetic order parameter¹⁸, though in this case there are insufficient data close to T_N to provide an unambiguous determination of β .

The form of the raw data for $\text{Ca}_5\text{Ir}_3\text{O}_{12}$ is more complicated. Though dominated by a single primary oscillation frequency, fitting with additional frequency components with smaller amplitudes (and frequencies ranging from 0.8–4 MHz) improved the quality of the fit, using up to four or five frequencies. Fig. 2 shows the data above and below the transition, together with a fit to the low temperature data using one and five frequencies for comparison. While the five frequency fit clearly succeeds in describing the data over a significantly longer time, the parameters of the smaller amplitude oscillations are not well defined and the frequencies could not be followed through to higher temperatures. The single frequency fit achieves a satisfactory and consistent parametrization of the largest amplitude oscillating component across the temperature range measured. These results indicate the existence of several magnetically inequivalent muon stopping sites.

The data set was analysed by fitting just to the frequency component with the largest amplitude, the precession frequency of which is shown in Fig. 2 and reaches ≈ 1.3 MHz as $T \rightarrow 0$. This precession frequency was fitted to Eq. (2), yielding $T_N = 7.84(7)$ K, $\nu(0) = 1.30(2)$ MHz, $\alpha = 2.8(5)$ and $\beta = 0.40(6)$, and these

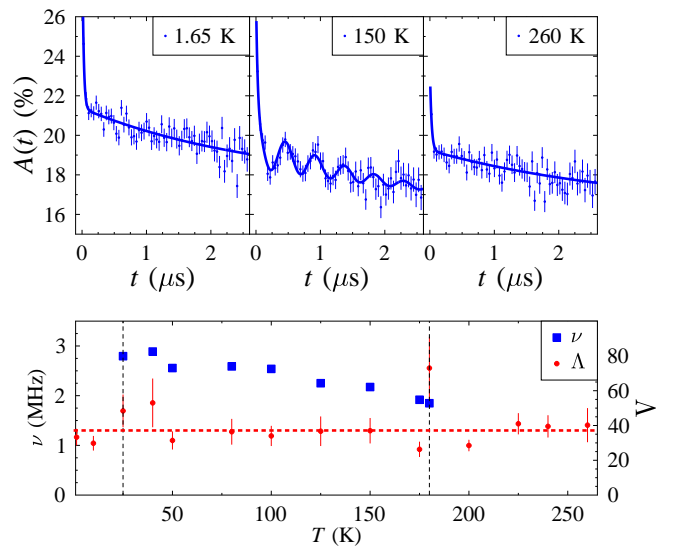


FIG. 3: (Color online) Data for $\text{Sr}_3\text{Ir}_2\text{O}_7$ in the three different phases of the material. The data in the intermediate phase was fitted with an oscillating component ν (blue squares) and a relaxing component Λ (red circles) [Eq. (3)]. The relaxation Λ (red circles) can be observed over the whole range of temperatures.

parameters are also consistent with three-dimensional behavior.

IV. Sr_2IrO_4 AND $\text{Sr}_3\text{Ir}_2\text{O}_7$

$\text{Sr}_3\text{Ir}_2\text{O}_7$ and Sr_2IrO_4 are both antiferromagnetic with transition temperatures T_N at 285 K (Ref. 5) and 240 K (Ref. 19), respectively. Both compounds contain Ir^{4+} ($S = \frac{1}{2}$) ions. In both compounds, a weak ferromagnetic moment is observed suggesting that they are both canted antiferromagnets^{6,13,20}.

$\text{Sr}_3\text{Ir}_2\text{O}_7$ belongs to the Ruddlesden-Popper series $\text{Sr}_{n+1}\text{Ir}_n\text{O}_{3n+1}$ with $n = 2$ and is constructed out of Ir-O bilayers with Sr-O interlayers⁵. Field cooled magnetization data picked up three anomalies, a kink at $T^* = 260$ K, a step downturn at $T_D = 50$ K and the magnetization becoming negative⁵ below about 20 K. These features were not observed in the zero-field-cooled magnetization data, implying a strong spin disordering or a random orientation of magnetic domains that persists through T_N . The transitions at T^* and T_D could also be identified in resistivity data, but no explanation for the comprehensive magnetization and transport behavior has been found so far⁵.

Sr_2IrO_4 is the $n = 1$ member of the Ruddlesden-Popper series (i.e. it has the K_2NiF_4 structure) and is therefore constructed out of single Ir-O layers with Sr-O interlayers²¹. The strong spin-orbit coupling acting on the t_{2g} manifold results in a filled $J = \frac{3}{2}$ lower band and a half-filled $J = \frac{1}{2}$ upper band. The narrow bandwidth

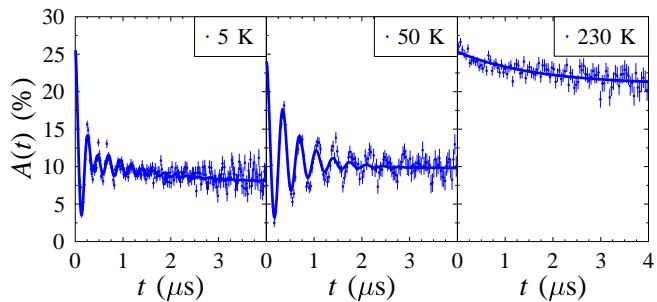


FIG. 4: (Color online) Raw data for Sr_2IrO_4 above and below the magnetic phase transition. The low temperature data was fitted with one relaxation component and two oscillating components [Eq. (1)], whereas for the data above 20 K we used a relaxing component and only one oscillating component [Eq. (3)].

of the upper band leads to a Mott insulating state, even though the electronic correlations (parametrized by U) are weaker than in more familiar Mott insulators, such as the underdoped cuprates. Sr_2IrO_4 can therefore be thought of as a spin-orbit induced Mott insulator^{6,22–24}. In addition, a metamagnetic transition occurs at 0.2 T, well below 240 K⁷. Chikara *et al.*⁸ have recently discovered another magnetic transition at 100 K, which is thought to be a reorientation transition of the spins.

The results of our μSR experiments on $\text{Sr}_3\text{Ir}_2\text{O}_7$ are summarized in Fig. 3 where the muon decay asymmetry for 1.5 K, 150 K and 260 K is presented. The presence of a fast relaxing component observed at short times can be taken to be a signature of magnetic order, but oscillations with a single precession frequency are only observed between 20 K and 160 K. In this temperature interval we fitted the data using

$$A(t) = A_1 \exp(-\lambda_1 t) \cos(2\pi\nu_1 t) + A_2 \exp(-\Lambda t). \quad (3)$$

The disappearance of the precession signal below 20 K is unusual and corresponds to the temperature at which the magnetization was observed to become negative⁵. We note that it was not possible to fit the frequency to Eq. (2) since the oscillations are only observed outside the critical region.

The data obtained for Sr_2IrO_4 show much richer behavior. The μSR spectra at three different temperatures are shown in Fig. 4. Above the magnetic ordering transition there is no oscillatory signal and, as is generally the case in paramagnets, the data are well described by an exponential relaxation. Between T_N and 20 K the data could be parametrized using one oscillation component and one exponentially relaxing component. Below 100 K the relaxation rates Λ and λ_1 both increase, the former quite sharply, and below 20 K a second frequency needs to be included for a satisfactory fit. The values obtained with this fitting procedure are plotted in Fig. 5. The higher of the two frequencies has a smaller amplitude and also has the smaller linewidth while the

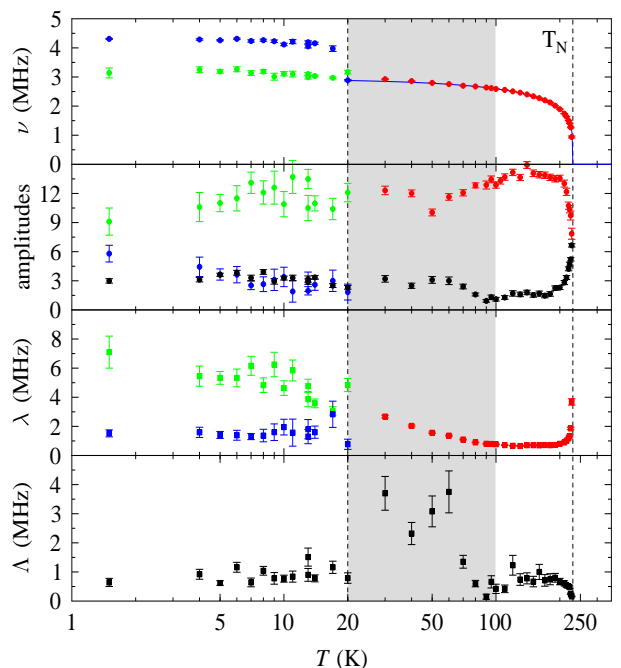


FIG. 5: (Color online) Fitted frequencies, amplitudes, linewidths and relaxation of Sr_2IrO_4 . The amplitudes and linewidths corresponding to the different components have been differentiated by color. The shaded region marks the temperature interval in which the relaxation rates increase on cooling, before the single precession frequency splits into two.

lower frequency is rather similar in magnitude to that observed in $\text{Sr}_3\text{Ir}_2\text{O}_7$, suggesting a rather similar muon site within the perovskite block in both compounds. As the temperature decreases in Sr_2IrO_4 the precession signal appears to evolve continuously in frequency, amplitude and relaxation rate, transforming into the lower frequency component seen in Fig. 5. The new component which appears below 20 K represents additional amplitude. The temperature interval in which the relaxation rates are growing upon cooling, just before the second frequency appears, is shown as a shaded region in Fig. 5. The single precession frequency was fitted with Eq. (2) in the temperature region from 20 K up to T_N and yields $T_N = 230.4(3)$ K, $\nu(0) = 2.93(1)$ MHz, $\alpha = 0.98(4)$ and $\beta = 0.21(1)$. Fitting just the data points close to T_N to the form $\nu(T) \propto (1 - T/T_N)^\beta$ yields $T_N = 228.2(1)$ K and $\beta = 0.19(1)$ (see Fig. 6 and inset). Both these estimates of β are consistent with a two-dimensional magnetic order parameter¹⁸.

V. DISCUSSION

The results of these experiments confirm the occurrence of antiferromagnetic order in Ca_4IrO_6 and $\text{Ca}_5\text{Ir}_3\text{O}_{12}$ and provide very accurate measurements of the Néel temperature in each case. The more complex

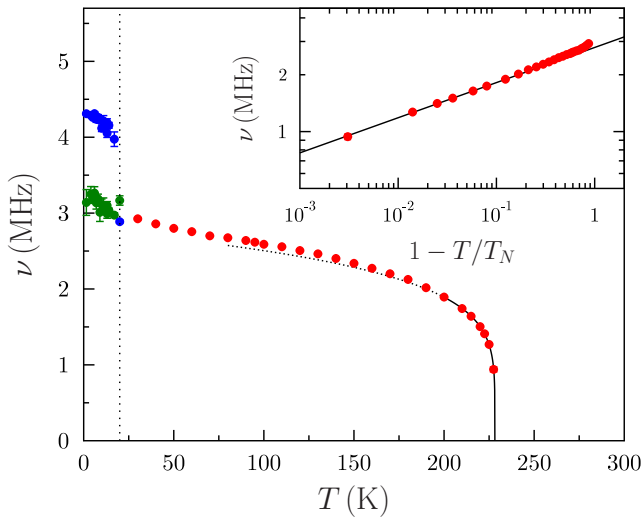


FIG. 6: (Color online) Temperature dependence of the fitted frequency observed in Sr_2IrO_4 . Inset: a fit of these data near T_N .

nature of the muon signal in $\text{Ca}_5\text{Ir}_3\text{O}_{12}$ as compared with that in Ca_4IrO_6 can be attributed to the larger number of magnetically inequivalent muon stopping sites. The presence of both Ir^{4+} and Ir^{5+} in $\text{Ca}_5\text{Ir}_3\text{O}_{12}$ means that the electronic moments are more dilute and this is consistent with the smaller magnitude of the internal field measured by the muons, almost half that found for Ca_4IrO_6 .

$\text{Sr}_3\text{Ir}_2\text{O}_7$ and Sr_2IrO_4 exhibit much more surprising and complicated behavior. In $\text{Sr}_3\text{Ir}_2\text{O}_7$ a single frequency was observed between 20 and 160 K. The disappearance

of precession below 20 K and above 160 K is mysterious. The change below 20 K does not correlate with any previously identified magnetic transition but corresponds to the temperature at which the field-cooled magnetization becomes negative.

Although the high temperature behavior of Sr_2IrO_4 is conventional, with the appearance of one frequency below the transition temperature at 260 K, the low temperature behavior is very unusual. Cooling below around 100 K induces a marked change in behavior, resulting in the development of a second precession signal which fully establishes below 20 K. It has previously been suggested⁸ that a reorientation transition occurs at 100 K in this material, and this is compatible with our data and correlates with a change in the Ir–O–Ir bond-angle. In this picture, the magnetic structure changes due to a temperature-induced change in couplings, and this causes two structurally equivalent muon sites to experience increasingly distinct local fields which lock in below 20 K. This development of a reoriented phase may be gradual (occurring over the shaded region of Fig. 5), which could result from the balance of competing energies changing with temperature. This reorientation of the spins to a lower symmetry state could be at the root of the magnetoelectric behavior⁸.

Acknowledgments

We thank EPSRC for financial support and Peter Battle for useful discussions. Part of this work was carried out at the Swiss Muon Source ($S\mu S$) and we are grateful to Alex Amato for technical support and Jack Wright for experimental assistance. GC was supported by NSF through grants DMR-0856234 and EPS-0814194.

-
- ¹ E. Dagotto, *Science* **309**, 257 (2005).
² M. Imada, A. Fujimori, and Y. Tokura, *Rev. Mod. Phys.* **70**, 1039 (1998).
³ G. Cao, V. Durairaj, S. Chikara, S. Parkin, and P. Schlottmann, *Phys. Rev. B* **75**, 134402 (2007).
⁴ M. Wakeshima, N. Taira, Y. Hinatsu, and Y. Ishii, *Solid State Commun.* **125**, 311 (2003).
⁵ G. Cao, Y. Xin, C. S. Alexander, J. E. Crow, P. Schlottmann, M. K. Crawford, R. L. Harlow, and W. Marshall, *Phys. Rev. B* **66**, 214412 (2002).
⁶ B. J. Kim, H. Jin, S. J. Moon, J. Y. Kim, B. G. Park, C. S. Leem, J. Yu, T. W. Noh, C. Kim, S. J. Oh, et al., *Phys. Rev. Lett.* **101**, 076402 (2008).
⁷ B. J. Kim, H. Ohsumi, T. Komesu, S. Sakai, T. Morita, H. Takagi, and T. Arima, *Science* **323**, 1329 (2009).
⁸ S. Chikara, O. Korneta, W. P. Crummett, L. E. DeLong, P. Schlottmann, and G. Cao, *Phys. Rev. B* **80**, 140407 (2009).
⁹ O. B. Korneta, T. Qi, S. Chikara, S. Parkin, L. E. De Long, P. Schlottmann, and G. Cao, *Phys. Rev. B* **82**, 115117 (2010).
¹⁰ F. Wang and T. Senthil (2010), arXiv:1011.3500v2.
¹¹ R. F. Sarkozy, C. W. Moeller, and B. L. Chamberland, *J. Sol. State Chem.* **9**, 242 (1974).
¹² N. Segal, J. F. Vente, T. S. Bush, and P. D. Battle, *J. Mat. Chem.* **6**, 395 (1996).
¹³ N. S. Kini, A. M. Strydom, H. S. Jeevan, C. Geibel, and S. Ramakrishnan, *J. Phys.: Condens. Matter* **18**, 8205 (2006).
¹⁴ S. J. Blundell, *Contemp. Phys.* **40**, 175 (1999).
¹⁵ F. J. J. Dijkema, J. F. Vente, E. Frikkee, and D. J. W. Ijdo, *Mater. Res. Bull.* **28**, 1145 (1993).
¹⁶ K. Hayashi, G. Demazeau, M. Pouchard, and P. Hagenmuller, *Mater. Res. Bull.* **15**, 461 (1980).
¹⁷ J. Darriet, G. Demazeau, and M. Pouchard, *Mater. Res. Bull.* **16**, 1013 (1981).
¹⁸ S. Blundell, *Magnetism in condensed matter* (Oxford University Press, Oxford, 2001).
¹⁹ G. Cao, J. Bolivar, S. McCall, J. E. Crow, and R. P. Guertin, *Phys. Rev. B* **57**, R11039 (1998).
²⁰ I. Nagai, Y. Yoshida, S. I. Ikeda, H. Matsuhata, H. Kito, and M. Kosaka, *J. Phys.: Condens. Matter* **19**, 136214 (2007).
²¹ M. K. Crawford, M. A. Subramanian, R. L. Harlow, J. A. Fernandez-Baca, Z. R. Wang, and D. C. Johnston, *Phys. Rev. B* **49**, 9198 (1994).

- ²² S. J. Moon, H. Jin, W. S. Choi, J. S. Lee, S. S. A. Seo, J. Yu, G. Cao, T. W. Noh, and Y. S. Lee, Phys. Rev. B **80**, 195110 (2009).
- ²³ H. Jin, H. Jeong, T. Ozaki, and J. Yu, Phys. Rev. B **80**,

- 075112 (2009).
- ²⁴ H. Watanabe, T. Shirakawa, and S. Yunoki, Phys. Rev. Lett. **105**, 216410 (2010).